CHAPTER IV

RESULTS AND DISCUSSION

4.1 Isolation of endophytic fungi

Sixty five and three endophytic fungal isolates were isolated from the twigs and leaves of the plant *Hydnocarpus anthelminthicus* Pierre ex., as shown in Table 4.1, respectively. Plant samples were collected from the Central Botanical Garden (Pukae), Saraburi Province, Thailand. Each fungus isolate was grown on six different culture media, including Malt Czapek Agar (MCzA), Malt Extract Agar (MEA), Potato dextrose agar (PDA), Sabouraud's Dextrose Agar (SDA), Yeast Czapek Agar (YCz), and Yeast Extract Sucrose Agar (YES), for 14 days at room temperature. The examples of colony morphology of isolated endophytic fungi are shown in Figure 4.1.

Table 4.1 Number of endophytic fungi isolated from *Hydnocarpus anthelminthicus* Pierre ex.

Plant section	Number of isolate
Twig	65
Leaves	3

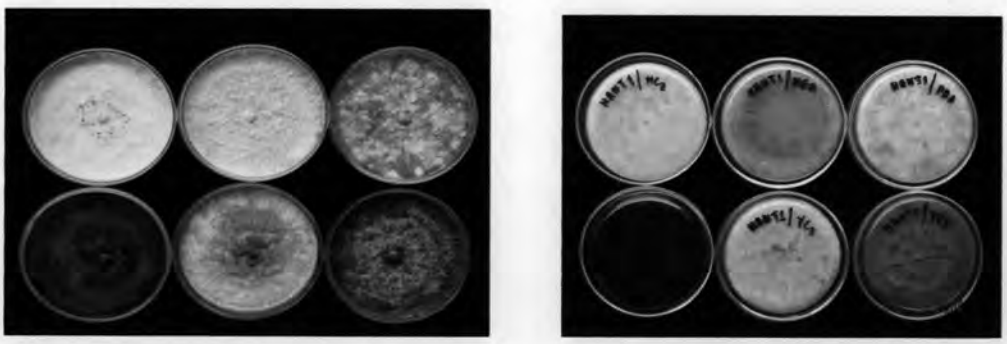

Obverse **Reverse**

Figure 4.1 Colonial morphology characteristics of endophytic fungal isolates HANT 1, on six media culture: top left, MCz; top middle, MEA; top right, PDA; bottom left, SDA; bottom middle, YCz; and bottom right, YES.

4.2 Screening of endophytic fungi for anti-*Candida albicans* activity

Sixty eight isolates of endophytic fungi were grown on MCzA, MEA, PDA, SDA, YCz, and YES at room temperature for 14 days. The screening of endophytic fungi for anti-*C. albicans* activity was by agar disk diffusion assay. The inhibition zones around the agar blocks of endophytic fungal isolates were observed, as shown in Table B1 in Appendix B, and the examples of inhibition zones are shown in Figure 4.2.

By agar disk diffusion assay, 13 isolates of endophytic fungi were found to passess anti-*Candida albicans* activity, 19 isolates were found synergistically with ketoconazole drug, and 14 isolates were found synergistically with nystatin drug.

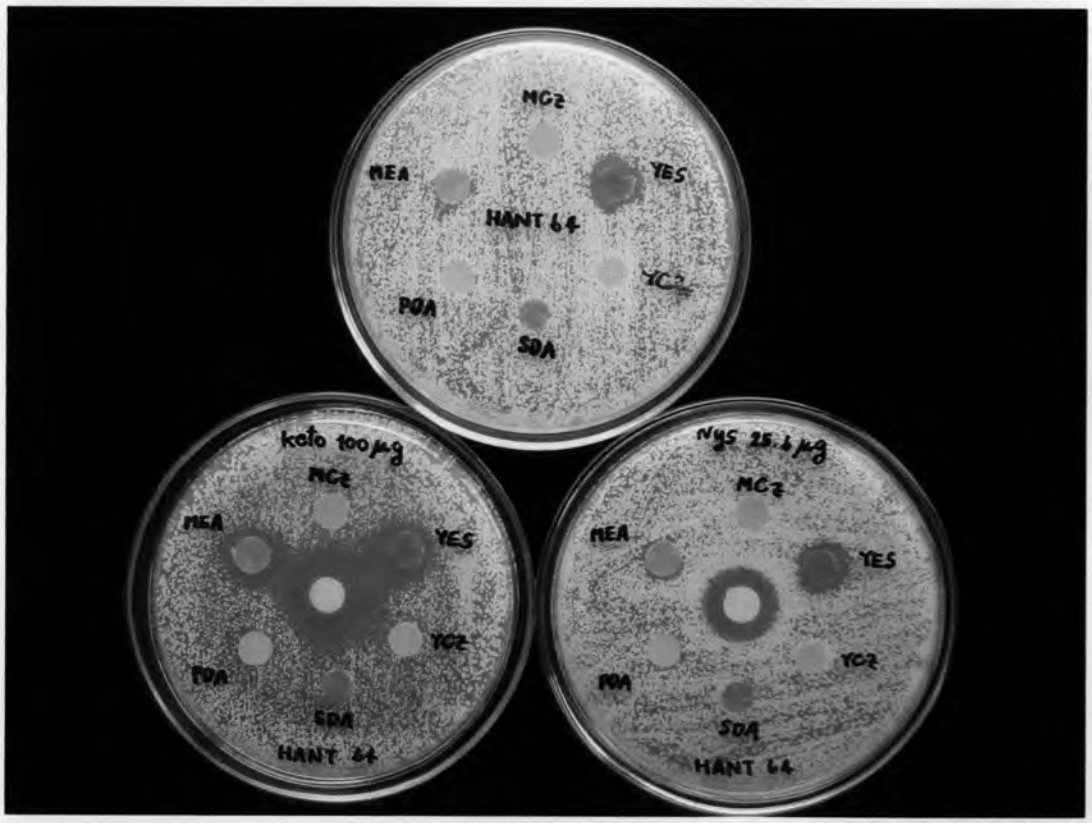

Figure 4.2 Agar disk diffusion assay testing the combination of ketoconazole and nystatin and endophytic fungal isolate HANT 64. The fungal agar blocks were placed onto inoculated agar plates. Cellulose disk impregnated with the ketoconazole (left lower) and nystatin (right lower) were placed onto the center of agar plate.

4.3 Structure elucidation of the isolated compounds from endophytic fungal isolates HANT 7 and HANT 25

4.3.1 Structure elucidation of compound 1

Compound **1** was obtained as a colorless needle from MeOH (126.8 mg, 14.1% yield), mp 189-190°C, $[\alpha]_D^{29}$ +303 (*c* 0.31, MeOH), UV (MeOH) λ_{max} 257 and 221 nm, and determined to have the molecular formula $C_{16}H_{18}O_5$ by ESI-TOFMS data (*m/z* 291.1232 $[M+H]^+$, calcd 291.1232 for $C_{16}H_{19}O_5$). The IR spectrum of compound **1** is shown in Figure C2 in appendix C, and the absorption peaks were assigned as displayed in Table 4.2.

Table 4.2 Assignments of the IR absorption bands of compound **1**.

Wave number (cm^{-1})	Intensity	Vibration
1738	Strong	C=O stretching vibration of esters
1719	Strong	C=O stretching vibration of α, β-unsaturated lactones
1366	Medium	C-H bending vibration of $-CH_3$ (alkanes)
1231	Strong	C-O stretching vibration of esters
1022	Strong	C-O-C stretching vibration of ethers
734, 691	Strong	C=CH out of plane vibration of alkenes

The ^1H NMR spectrum of compound **1** in $CDCl_3$ (Figures C1 and C2 in appendix C, Table 4.3) displayed a total of 14 signals, including two methyl groups at 2.03 (3H, s, H-16) and 1.14 (3H, d, *J* = 6.8 Hz, H-14), six double-bond protons at 7.04 (1H, dd, *J* = 9.7 and 6.0 Hz, H-3), 6.23 (1H, d, *J* = 9.7 Hz, H-2), 6.10 (1H, m, H-11), 6.03 (1H, m, H-8), 5.92 (1H, m, H-10), and 5.90 (1H, m, H-9), four carbinols at 5.09 (1H, dd, *J* = 6.0 and 2.4 Hz, H-4), 4.52 (1H, t, *J* = 5.8 Hz, H-7), 4.51 (1H, dd, *J* = 11.0 and 2.4 Hz, H-5), and 4.29 (1H, d, *J* = 4.5 Hz, H-12), and two methines at 3.05 (1H, m, H-6) and 3.01 (1H, m, H-13).

The ^{13}C NMR spectrum of compound **1** ($CDCl_3$) (Figure C5 in appendix C, Table 4.3), together with HMQC (Figure C7 in appendix C) and DEPT (Figure C6 in appendix C) experiments, revealed the presence of two carbonyl carbon signals (δ_C

170.0, 162.2), six olefinic carbon signals (δ_C 140.2, 137.4, 136.9, 126.2, 124.9, 124.4), four methine bearing oxygen signals (δ_C 86.3, 77.6, 75.8, 63.1), two methine signals (δ_C 52.6, 50.5), and two methyl groups (δ_C 20.6, 14.1). The compound **1** consisted of two major fragments; α,β-unsaturated δ-lactone and eight-membered ring.

An α,β-unsaturated δ-lactone substructure was elucidated by analyses of ^1H-^{13}C (HMBC) and ^1H-^1H COSY connectivities (Figure 4.3, Table 4.3). The ^1H-^1H COSY spectrum (Figure C8 in appendix C) demonstrated correlations from olefinic proton doublet at δ_H 6.23, (H-2) to a down-field proton (δ_H 7.04, H-3). The doublet-of-doublets at δ_H 7.04 (H-3) also coupled to a carbinol proton (δ_H 5.09, H-4), which in turn coupled to another carbinol proton (δ_H 4.51, H-5). The HMBC spectrum (Figures C9-C14 in appendix C) demonstrated correlations from H-3 to a carbonyl carbon at δ_C 162.2 (C-1), and the attachment of the acetyl group to C-4 of the lactone ring was evident from the long-range correlation from of H-4 to the down-field carbonyl (δ_C 170.0).

The partial structure of eight-membered ring could be grouped in pairs, according to like chemical shifts and multiplicity. The ^1H-^1H COSY spectrum demonstrated correlations from two carbinol protons at δ_H 4.52 (H-7) and δ_H 4.29 (H-12) to methine protons at δ_H 3.05 (H-6) and δ_H 3.01 (H-13), respectively and also correlated to olefinic protons at δ_H 6.03 (H-8) and δ_H 6.10 (H-11), respectively. The double bond protons at δ_H 5.90 (H-9) and δ_H 5.92 (H-10) correlated to two olefinic protons at δ_H 6.03 (H-8) and δ_H 6.10 (H-11), respectively.

An ether bridge between C-7 and C-12 was corroborated by the HMBC correlation of H-7 to C-12 and H-12 to C-7. The connectivity of the methyl group (δ_H 1.14, H-14) and the α,β-unsaturated δ-lactone to the C-13 and C-6 position of the cyclooctadiene, was established with the help of the COSY spectrum, showing methine proton (δ_H 3.01, H-13) correlated to methyl-proton doublet (δ_H 1.14, H-14) and methine proton (δ_H 3.05, H-6) correlated to carbinol proton (δ_H 4.51, H-5) of the lactone ring. These connections were supported by HMBC spectrum, showing the correlations of H-6, H-12, and H-13 to C-14 (methyl carbon); and H-6 to C-5 and C-4 of the lactone ring.

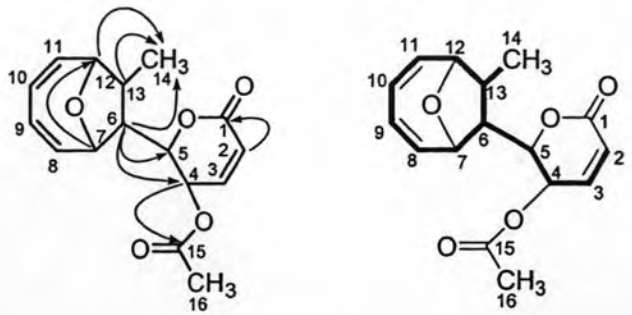

HMBC

-Bold lines are from the ^{1}H-^{1}H COSY correlations.

Figure 4.3 HMBC and ^{1}H-^{1}H COSY correlations of compound **1**.

Table 4.3 The ^{1}H, ^{13}C, multiplicity, COSY, and HMBC spectroscopic data of compound **1**.

Position	δ_C	δ_H	Multiplicity ($J_{H/H}$ Hz)	COSY (H to H)	HMBC (H to C)
1	162.2 (qC)	-	-	-	-
2	124.4 (CH)	6.23	d (9.7)	3	1,4
3	140.2 (CH)	7.04	dd (9.7, 6.0)	2,4	1,4,5
4	63.1 (CH)	5.09	dd (6.0, 2.4)	3,5	2,3,5,15
5	77.6 (CH)	4.51	dd (11, 2.4)	4,6	4,6,13
6	50.0 (CH)	3.05	m	5,7,13	4,5,7,8,13,14
7	75.8 (CH)	4.52	t (5.8)	6,8	5,6,8,9,12,13
8	136.9 (CH)	6.03	m	7,9	6,7,10
9	126.2 (CH)	5.90	m	8,10	7,11
10	124.9 (CH)	5.92	m	9,11	8,12
11	137.4 (CH)	6.10	m	10,12	9,10,12
12	86.3 (CH)	4.29	d (4.5)	11,13	6,7,10,11,13,14
13	52.6 (CH)	3.01	m	6,12,14	6,7,14
14	14.1 (CH_3)	1.14	d (6.8)	13	6,12,13
15	170.0 (qC)	-	-	-	-
16	20.6 (CH_3)	2.03	s	-	15

The relative configuration of compound **1** could be established by analyses of the NOESY spectrum (Figure C15 in appendix C, Figure 4.4), showing the correlations of H-4 to H-5 and H-7; H5 to H-7 and H-14; and H-7 to H-14.

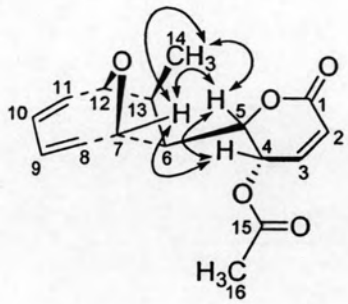

Figure 4.4 NOESY correlations of compound **1**.

On the basis of these spectroscopic data, the structure of compound **1** was elucidated as a known compound, namely mycoepoxydiene, previously isolated from the solid-state fermentation of a rare fungus designated as OS-F66617 (Cai *et al.*, 1999). Comparison of ^{1}H, ^{13}C NMR, and HMBC data of mycoepoxydiene and compound **1** is shown in Table 4.4.

Table 4.4 The ^{1}H, ^{13}C, and HMBC spectroscopic data of mycoepoxydiene and compound **1**.

Mycoepoxydiene (Cai *et al.*, 1999)				**Compound 1**		
Position	δ_C	δ_H	**HMBC (H to C)**	δ_C	δ_H	**HMBC (H to C)**
1	162.2	-	-	162.2	-	-
2	125.1	6.23	1,4	124.4	6.23	1,4
3	140.2	7.02	4,5	140.2	7.04	1,4,5
4	63.3	5.05	2,5,15	63.1	5.09	2,3,5,15
5	77.8	4.47	4,6,13	77.6	4.51	4,6,13
6	50.2	3.03	4,5,7,8,13,14	50.0	3.05	4,5,7,8,13,14
7	76.0	4.27	5,6,8,9,12,13	75.8	4.52	5,6,8,9,12,13
8	137.0	6.02	6,7,9	136.9	6.03	6,7,10
9	126.3	5.88	6,7,11	126.2	5.90	7,11,
10	124.5	5.90	8,12	124.9	5.92	8,12
11	137.8	6.08	12	137.4	6.10	9,10,12
12	86.6	4.31	6,7,10,11,13,14	86.3	4.29	6,7,10,11,13,14
13	52.8	3.01	6,7,11,14	52.6	3.01	6,7,14
14	14.5	1.12	6,12,13	14.1	1.14	6,12,13
15	170.0	-	-	170.0	-	-
16	21.0	2.01	15	20.6	2.03	15

4.3.2 Structure elucidation of compound 2

Compound **2** was obtained as a white feather-like crystal (7.5 mg, 0.8% yield), $[\alpha]_D^{30}$ +80 (*c* 0.60, MeOH), UV (MeOH) λ_{max} (log ε) 264 (3.60) and 222 (3.52) nm, and determined to have the molecular formula $C_{14}H_{16}O_4$ by ESI-TOFMS data (*m/z* 249.1117 $[M+H]^+$ calcd 249.1127 for $C_{14}H_{17}O_4$). The IR spectrum of compound **2** is shown in Figure C17 in appendix C and the absorption peaks were assigned as displayed in Table 4.5.

Table 4.5 Assignments of the IR absorption bands of compound **2**.

Wave number (cm^{-1})	Intensity	Vibration
3351	Medium	O-H stretching vibration of hydroxyl group
1714	Strong	C=O stretching vibration of α, β-unsaturated lactones
1380	Medium	C-H bending vibration of $-CH_3$ (alkanes)
1259	Strong	C-O stretching vibration of esters
1018	Strong	C-O-C stretching vibration of ethers
691	Strong	C=CH out of plane vibration of alkenes

The ^{1}H NMR spectrum of compound **2** ($CDCl_3$) (Figures C18 and C19 in appendix C, Table 4.6) displayed a total of 13 signals, including one methyl group at 1.14 (3H, d, *J* = 6.96 Hz, H-14), six double-bond protons at 7.05 (1H, dd, *J* = 9.7 and 6.0 Hz, H-3), 6.26 (1H, m, H-8), 6.14 (1H, d, *J* = 9.7 Hz, H-2), 6.13 (1H, m, H-11), 5.97 (1H, m, H-9), and 5.92 (1H, m, H-10), four carbinols at 4.44 (1H, t, *J* = 5.6 Hz, H-7), 4.35 (1H, dd, *J* = 10.6 and 2.4 Hz, H-5), 4.33 (1H, bd, *J* = 2.5 Hz, H-12), and 4.09 (1H, dd, *J* = 6.1 and 2.3 Hz, H-4), and two methines at 3.06 (1H, ddd, *J* = 10.6, 7.0, and 5.6 Hz, H-6), and 2.98 (1H, qn d, *J* = 6.7 and 1.3 Hz, H-13).

The ^{13}C NMR (Figure C20 in appendix C, Table 4.6), HMQC (Figure C22 in appendix C), and DEPT (Figure C21 in appendix C) spectrum of compound **2** ($CDCl_3$) were assigned to one carbonyl carbon signal (δ_C 163.1), six olefinic carbon signals (δ_C 144.1, 137.3, 137.2, 126.3, 124.8, 123.1), four methine bearing oxygen signals (δ_C 86.1, 79.3, 76.8, 62.0), two methine signals (δ_C 51.7, 51.6), and one methyl groups (δ_C 14.2).

Table 4.6 The ^{1}H, ^{13}C, multiplicity, and HMBC spectroscopic data of compound **2**.

Position	δ_C	δ_H	Multiplicity ($J_{H/H}$ Hz)	COSY (H to H)	HMBC (H to C)
1	163.1 (qC)	-	-	-	-
2	123.1 (CH)	6.14	d (9.7)	3	1,4
3	144.1 (CH)	7.05	dd (9.7, 6.0)	2,4	1,4,5
4	62.0 (CH)	4.09	dd (6.1, 2.3)	3,5	2,3,5
5	79.3 (CH)	4.35	d (2.2)	4,6	4,6,7,13
6	51.7 (CH)	3.06	ddd (10.6, 7.0, 5.6)	5,7,13	4,5,7,8,13,14
7	76.8 (CH)	4.44	t (5.6)	6,8	5,6,8,9,12,13
8	137.2 (CH)	6.26	m	7,9	7,10
9	126.3 (CH)	5.97	m	8,10	7,8,11
10	124.8 (CH)	5.92	m	9,11	8,11,12
11	137.3 (CH)	6.13	m	10,12	9,10,12
12	86.1 (CH)	4.33	bd (2.5)	11,13	6,7,11,13,14
13	51.6 (CH)	2.98	qn d (7.0, 1.3)	6,12,14	6,7,11,14
14	14.2 (CH_3)	1.14	d (7.0)	13	6,12,13

The ^{1}H and ^{13}C NMR data for compound **2** were very similar to those of compound **1**, suggesting that the two molecules were closely related (Table 4.7). The difference of the ^{1}H NMR spectrum of compound **2** from that of compound **1** was the absence of an acetyl group signal (δ_H 2.03).

In addition, the IR spectrum of compound **2** showed the absorption band of a hydroxy group at 3351 cm^{-1}, and the ESI-TOFMS data suggested that the acetyl group in compound **1** was replaced by the hydroxy group in compound **2**.

Table 4.7 The ^{1}H, ^{13}C, and HMBC spectroscopic data of compounds **1** and **2**.

	Compound 1			Compound 2		
Position	δ_C	δ_H	**HMBC (H to C)**	δ_C	δ_H	**HMBC (H to C)**
1	162.2	-	-	163.1	-	-
2	124.4	6.23	1,4	123.1	6.14	1,4
3	140.2	7.04	1,4,5	144.1	7.05	1,4,5
4	63.1	5.09	2,3,5,15	62.0	4.09	2,3,5
5	77.6	4.51	4,6,13	79.3	4.35	4,6,7,13
6	50.0	3.05	4,5,7,8,13,14	51.7	3.06	4,5,7,8,13,14
7	75.8	4.52	5,6,8,9,12,13	76.8	4.44	5,6,8,9,12,13
8	136.9	6.03	6,7,10	137.2	6.26	7,10
9	126.2	5.90	7,11,	126.3	5.97	7,8,11
10	124.9	5.92	8,12	124.8	5.92	8,11,12
11	137.4	6.10	9,10,12	137.3	6.13	9,10,12
12	86.3	4.29	6,7,10,11,13,14	86.1	4.33	6,7,11,13,14
13	52.6	3.01	6,7,14	51.6	2.98	6,7,11,14
14	14.1	1.14	6,12,13	14.2	1.14	6,12,13
15	170.0	-	-	-	-	-
16	20.6	2.03	15	-	-	-

Structure of compound **2** was elucidated by analyses of ^{1}H-^{13}C (HMBC), HMQC, and ^{1}H-^{1}H COSY spectra (Figure C23 in appendix C, Table 4.6). The compound **2** consisted of two major fragments; α,β-unsaturated δ-lactone and eight-membered ring.

The ^{1}H-^{1}H COSY spectrum (Figure 4.5) illustrated the linkage from a doublet-of-doublets at δ_H 7.05 (H-3) to olefinic proton doublet at δ_H 6.14, (H-2) and a

carbinol proton at δ_H 4.09 ppm (H-4) and H-4 coupled to a carbinol proton at δ_H 4.34 (H-5). The HMBC spectrum (Figure 4.5) demonstrated correlation from H-2 to a carbonyl carbon at δ_C 163.1 (C-1).

Further analysis of the COSY and HMBC correlations established the eight- membered ring of **2**. The COSY spectrum showed the connectivity from H-6 through H-14. The HMBC spectrum showed an ether bridge between C-7 and C-12 by the long-range ^1H-^{13}C correlations of H-7 to C-12 and H-12 to C-7.

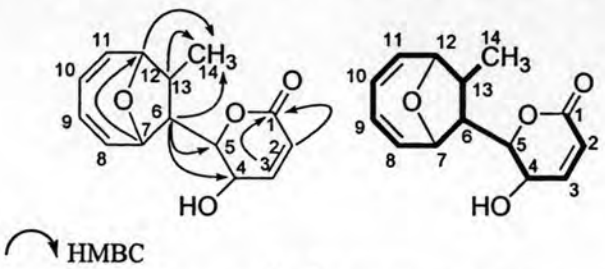

Figure 4.5 HMBC and ^1H-^1H COSY correlations of compound **2.**

The relative configuration of compound **2** could be established by analyses of the NOESY spectrum (Figure C29 in appendix C), showing the correlations of H-4 to H-5 and H-7; H5 to H-7 and H-14, and H-7 to H-14. The relative configuration of compound **2** is shown in Figure 4.6.

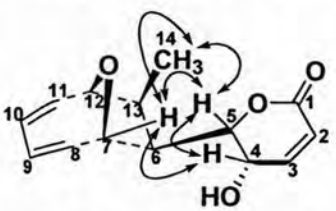

Figure 4.6 NOESY correlations of compound **2**.

Based upon these spectroscopic data, the structure of compound **2** was elucidated as a new natural products compound, previously been synthesised from the asymmetric total synthesis (Takao *et al.*, 2004).

4.3.3 Structure elucidation of compound 3

Compound **3** was obtained as a colorless needle (2.1 mg, 0.2% yield), $[\alpha]_D^{22}$ +21 (*c* 0.18, MeOH), UV (MeOH) λ_{max} (log ε) 258 (3.52), and determined to have the molecular formula $C_{14}H_{16}O_4$ by ESI-TOFMS data (*m/z* 293.1389 $[M+H]^+$, calcd 293.1389 for $C_{16}H_{21}O_5$). The IR spectrum of compound **3** is shown in Figure C31 in appendix C and the absorption peaks were assigned as displayed in Table 4.8.

Table 4.8 Assignments of the IR absorption bands of compound **3**.

Wave number (cm^{-1})	Intensity	Vibration
2921	Strong	C-H stretching vibration of alkanes
1733	Strong	C=O stretching vibration of lactones
1457, 1437, 1373	Medium	C-H bending vibration of $-CH_3$, $-CH_2$ (alkanes)
1235	Strong	C-O stretching vibration of esters
1041	Strong	C-O-C stretching vibration of ethers
694	Strong	C=CH out of plane vibration of alkenes

The ^1H NMR spectrum of compound **3** in $CDCl_3$ (Figures C31 and C32 in appendix C, Table 4.9) displayed a total of 14 signals, including two methyl groups at 2.04 (3H, s, H-16) and 1.12 (3H, d, J = 6.9 Hz, H-14), four double-bond protons at 6.07 (1H, m, H-11), 6.06 (1H, m, H-8), 5.90 (1H, m, H-10), and 5.88 (1H, m, H-9), four carbinols at 5.05 (1H, m, H-4), 4.38 (1H, dd, J = 11.0 and 1.4 Hz, H-5), 4.30 (1H, d, J = 4.4 Hz, H-12), and 4.26 (1H, t, J = 6.0 Hz, H-7), two methylenes at 2.59 (2H, dd, J = 6.0 and 2.8 Hz, H-2) and 2.18 (2H, m, H-3), and two methines at 2.96 (1H, qn, J =7.0 Hz, H-13) and 2.91 (1H, dt, J = 11.0 and 6.7 Hz, H-6).

The ^{13}C NMR spectrum of compound **3** in $CDCl_3$, (Figure C34 in appendix C, Table 4.9) exhibited 16 signals, and analyses of HMQC (Figure C36 in appendix C), and DEPT (Figure C35 in appendix C) spectra suggested the presence of two carbonyl carbons (δ_C 170.1, 169.4), four olefinic carbons (δ_C 137.5, 137.3, 126.1, 124.4), four methine bearing oxygen signals (δ_C 86.4, 79.5, 75.9, 66.7), two methine signals (δ_C 52.6, 51.2), two methylene signals (δ_C 25.2, 25.1), and two methyl groups (δ_C 21.0, 14.1).

Table 4.9 The ^{1}H, ^{13}C, multiplicity, and HMBC spectroscopic data of compound **3**.

Position	δ_C	δ_H	Multiplicity ($J_{H/H}$ Hz)	COSY (H to H)	HMBC (H to C)
1	169.4 (qC)	-	-	-	-
2	25.2 (CH_2)	2.59	dd (6.0, 2.8)	3	1,3,4
3	25.1 (CH_2)	2.18	m	2,4	1,2,4,5
4	66.7 (CH)	5.05	m	3,5	2,3,5,15
5	79.5 (CH)	4.38	dd (11.0, 1.4)	4,6	3,4,6,7,13
6	51.2 (CH)	2.91	dt (11.1, 6.7)	5,7,13	4,5,7,8,13,14
7	75.9 (CH)	4.26	t (6.0)	6,8	5,6,8,9,12,13
8	137.3 (CH)	6.06	m	7,9	6,7,9,10
9	126.1 (CH)	5.88	m	8,10	7,11
10	124.4 (CH)	5.90	m	9,11	8,12
11	137.5 (CH)	6.07	m	10,12	9,10
12	86.4 (CH)	4.30	d (4.4)	11	6,7,10,11,13,14
13	52.6 (CH)	2.96	qn (7.0)	6,12,14	6,7,11,14
14	14.1 (CH_3)	1.12	d (7.0)	13	6,12,13
15	170.1 (qC)	-	-	-	-
16	21.0 (CH_3)	2.04	s	-	15

The comparison of ^{1}H and ^{13}C NMR data of compound **3** with compound **1** is shown in Table 4.10. Both ^{1}H and ^{13}C NMR spectroscopic data of compound **3** were almost identical to those of compound **1,** except the absence of the two olefinic carbons at δ_C 124.4 and 140.2 ppm of the δ-lactone ring with additional two methylene carbons at δ_C 25.2 and 25.1 ppm (C-2 and C-3).

Table 4.10 The ^{1}H, ^{13}C, and HMBC spectroscopic data of compounds **1** and **3**.

	Compound 1			Compound 3		
Position	δ_C	δ_H	**HMBC (H to C)**	δ_C	δ_H	**HMBC (H to C)**
1	162.2	-	-	169.4	-	-
2	124.4	6.23	1,4	25.2	2.59	1,3,4
3	140.2	7.04	1,4,5	25.1	2.18	1,2,4,5
4	63.1	5.09	2,3,5,15	66.7	5.05	2,3,5,15
5	77.6	4.51	4,6,13	79.5	4.38	3,4,6,7,13
6	50.0	3.05	4,5,7,8,13,14	51.2	2.91	4,5,7,8,13,14
7	75.8	4.52	5,6,8,9,12,13	75.9	4.26	5,6,8,9,12,13
8	136.9	6.03	6,7,10	137.3	6.06	6,7,9,10
9	126.2	5.90	7,11,	126.1	5.88	7,11
10	124.9	5.92	8,12	124.4	5.90	8,12
11	137.4	6.10	9,10,12	137.5	6.07	9,10
12	86.3	4.29	6,7,10,11,13,14	86.4	4.30	6,7,10,11,13,14
13	52.6	3.01	6,7,14	52.6	2.96	6,7,11,14
14	14.1	1.14	6,12,13	14.1	1.12	6,12,13
15	170.0	-	-	170.1	-	-
16	20.6	2.03	15	21.0	2.04	15

The structure of compound **3** was established by analyses of HMQC, ^{1}H-^{13}C (HMBC) and ^{1}H-^{1}H COSY spectra (Figure C37 in appendix C, Table 4.9). Compound **3** consisted of 2 fragments; the δ-lactone moiety and eight membered ring.

The δ-lactone moiety was supported by ^{1}H-^{1}H COSY (Figure 4.7) and HMBC spectra (Figures C38-C44 in appendix C). The COSY spectrum showed the correlation from a doublet-of-doublets at δ_H 2.59 (H-2) to a methylene proton (δ_H 2.18, H-3). The methylene proton (H-3) also coupled to a carbinol proton (δ_H 5.05, H-

4), which in turn coupled to another carbinol proton (δ_H 4.38, H-5). The HMBC spectrum demonstrated a correlation from H-3 to a carbonyl carbon at δ_C 169.4 (C-1), and the attachment of the acetyl group to C-4 of the lactone ring was supported by the long-range correlation of H-4 to the down-field carbonyl (δ_C 170.1, C-15).

The partial structure of an eight-membered ring was assembled based on the following COSY and HMBC correlations. The ^1H-^1H COSY spectrum well established the connectivity from H-6 through H-14. In addition, an ether bridge between C-7 and C-12 was corroborated by the long range ^1H-^{13}C correlations of H-7 to C-12 and H-12 to H-7.

These connections were supported by the HMBC spectrum, showing the correlations of H-6, H-12, and H-13 to C-14 (methyl carbon), and H-6 to C-5 and C-4 of the lactone ring.

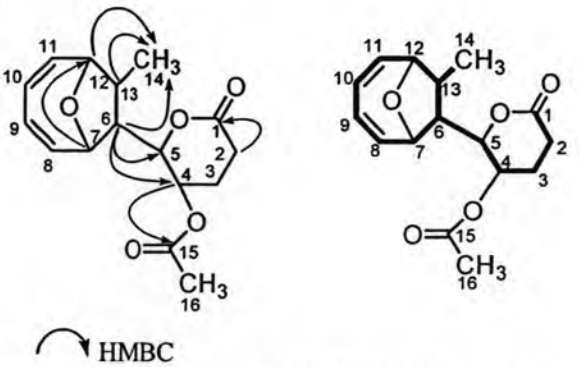

-Bold lines are from the ^1H-^1H COSY correlations.

Figure 4.7 HMBC and ^1H-^1H COSY correlations of compound **3**.

The relative configuration of compound **3** could be established by analyses of the NOESY spectrum (Figure C45 in appendix C), showing the correlations of H-4 to H-5 and H-7; H-5 to H-7 and H-14, and H-7 to H-14. The relative configuration of compound **3** is shown in Figure 4.8.

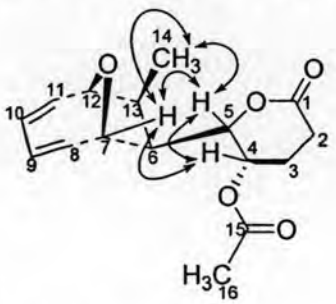

Figure 4.8 NOESY correlations of compound **3**.

4.3.4 Structure elucidation of compound 4

Compound **4** was obtained as a brown oil (17.4 mg, 1.9% yield) and determined to have the molecular formula $C_6H_8O_3$ by GC-MS data (*m/z* = 128).

The ^1H NMR spectrum of compound **4** (acetone-d_6) (Figure C47 in appendix C, Table 4.11) displayed 2 signals, an sp^2 methine proton at 6.18 (1H, s, H-3 and H-4) and a methylene proton at 4.47 (2H, s, H-6 and H-7).

The ^{13}C NMR spectrum of compound **4** (acetone-d_6) (Figure C48 in appendix C, Table 4.11) revealed the presence of a quaternary, olefinic, and methylene bearing oxygen carbons.

Table 4.11 The ^1H, ^{13}C and HMBC spectroscopic data of compound **4**.

Position	δ_C	δ_H	Multiplicity ($J_{H/H}$ Hz)	COSY (H to H)	HMBC (H to C)
2, 5	155.0 (qC)	-	-	-	-
3, 4	107.4 (CH)	6.18	s	-	2, 5, 6, 7
6, 7	56.4 (CH_2)	4.47	s	-	2, 5

Analyses of HMQC (Figure C50 in appendix C), DEPT (Figure C49 in appendix C) and mass spectroscopic data indicated three pairs of equivalent signals at δ_C 155.0, 107.4 and 56.4 ppm, suggesting the presence of a plane of symmetry in compound **4.** The HMBC spectrum (Figure C51 in appendix C, Table 4.11) demonstrated the correlations from H-3 to C-2 (or C-5) and C-6 (or C-7) and from methylene proton (H-6 or H-7) to C-2 (or C-5) (Figure 4.9).

On the basis of these spectroscopic data, the structure of compound **4** was elucidated as a known compound, namely 2,5-furandimethanol, previously isolated from *Streptomyces* sp. GW3/1538 (Mahmoud 2003), *Xylaria longipes*, and other fungi (Schneider *et al.*, 1996). 2,5-Furandimethanol has a moderate antimicrobial activity especially against fungi, *Nematospora coryli* and the yeast *Saccaromyces cerevisiae* (Mahmoud 2003).

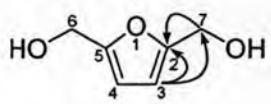

Figure 4.9: HMBC correlations of compound **4**.

4.4 Classification of the endophytic fungal isolates HANT 7 and HANT 25

4.4.1 Conventional method

4.4.1.1 Macroscopic morphology of the endophytic fungal isolates HANT 7 and HANT 25

Fungal isolates HANT 7 and HANT 25 did not produce conidia or spore on six different culture media (MCz, MEA, PDA, SDA, YCz, and YES), therefore, fungal isolates HANT 7 and HANT 25 were classified by microscopic morphology and molecular methods. Colony morphology of fungal isolates HANT 7 and HANT 25 are shown in Figures 4.10 and 4.11, respectively.

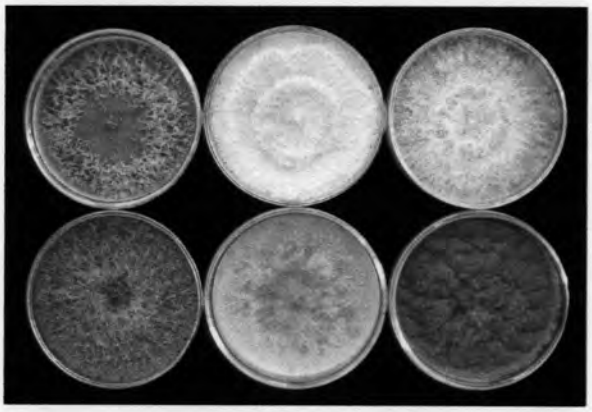

Obverse

Reverse

Figure 4.10 Colonial morphological characteristics of endophytic fungus isolate HANT 7 on six media culture: top left, MCz; top middle, MEA; top right, PDA; bottom left, SDA; bottom middle, YCz; and bottom right, YES.

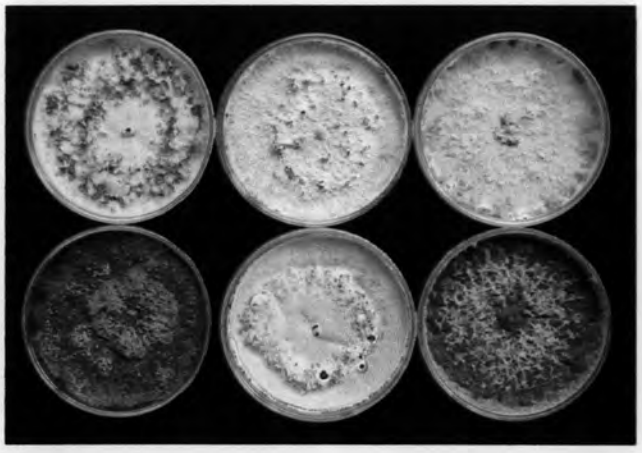

Obverse

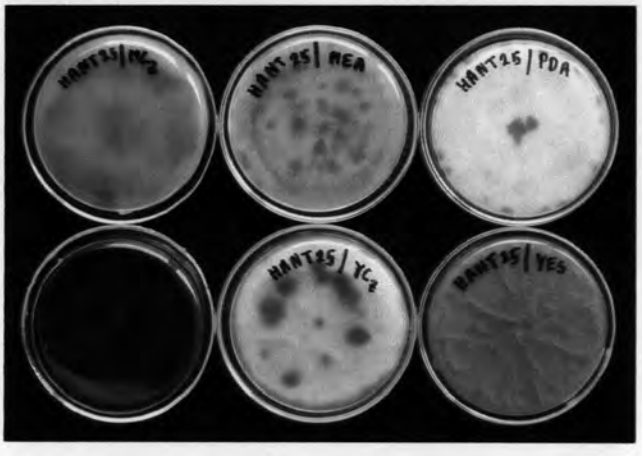

Reverse

Figure 4.11 Colonial morphological characteristics of endophytic fungus isolate HANT 25 on six media culture: top left, MCz; top middle, MEA; top right, PDA; bottom left, SDA; bottom middle, YCz; and bottom right, YES.

4.4.1.2 Microscopic morphology of the endophytic fungal isolates HANT 7 and HANT 25

On banana leaf agar, the fungal isolates HANT 7 and HANT 25 developed black pycnidia with two morphological distinct conidia, α-conidia and β-conidia. It was found that isolate HANT 7 and HANT 25 produced α-conidia in common rather than β-conidia that were infrequently found. Figures 4.12 and 4.13 show α-conidia of the isolates HANT 7 and HANT 25, respectively. Based on its

microscopic morphology, fungal isolates HANT 7 and HANT 25 were of the genera *Phomopsis* sp.

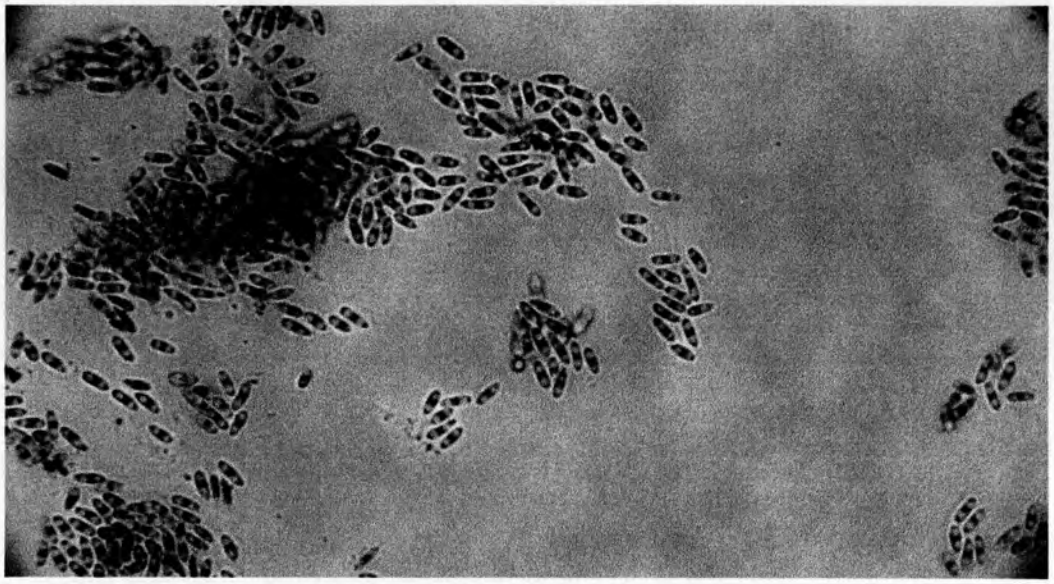

Figure 4.12 α-conidia of endophytic fungus isolate HANT 7.

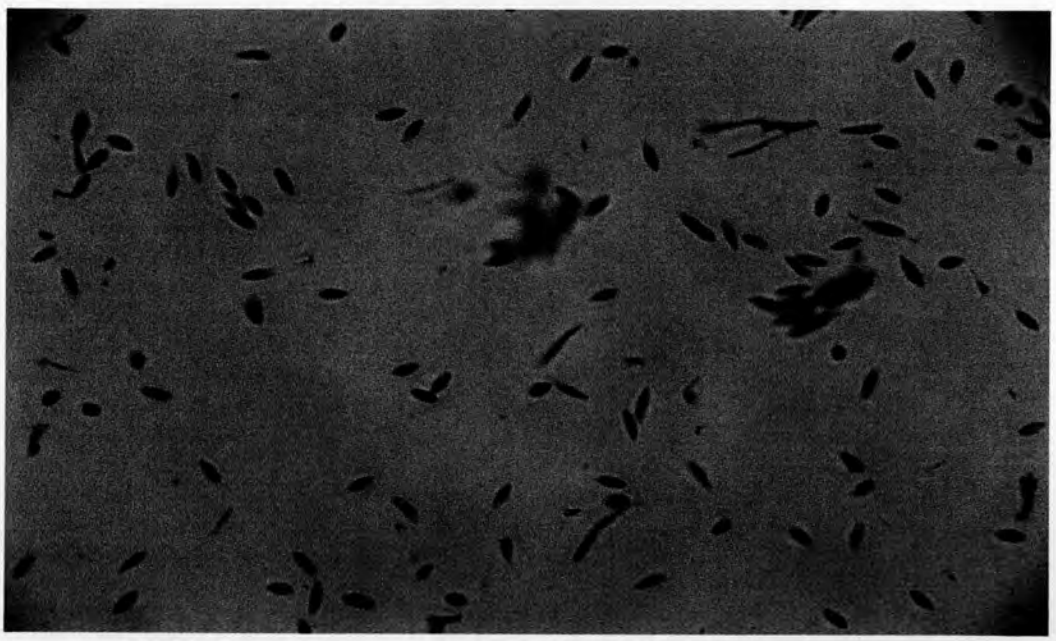

Figure 4.13 α-conidia of endophytic fungus isolate HANT 25.

4.4.2 Molecular Identification

4.4.2.1 Nucleotide sequence of complete ITS1-5.8S-ITS2 sequence of HANT 7

The ITS1-5.8S-ITS2 sequence of ribosomal DNA (rDNA) of isolate HANT 7 was amplified by PCR using the forward primer ITS5 and the reverse primer ITS4. Sequencing of the PCR product was performed at the Bioservice Unit (BSU), the National Center for Genetic Engineering and Biotechnology (BIOTEC). The length of a corresponding fragment was 490 bp, containing a part of the ITS1-5.8S-ITS2 rDNA (shown in Figure 4.14).

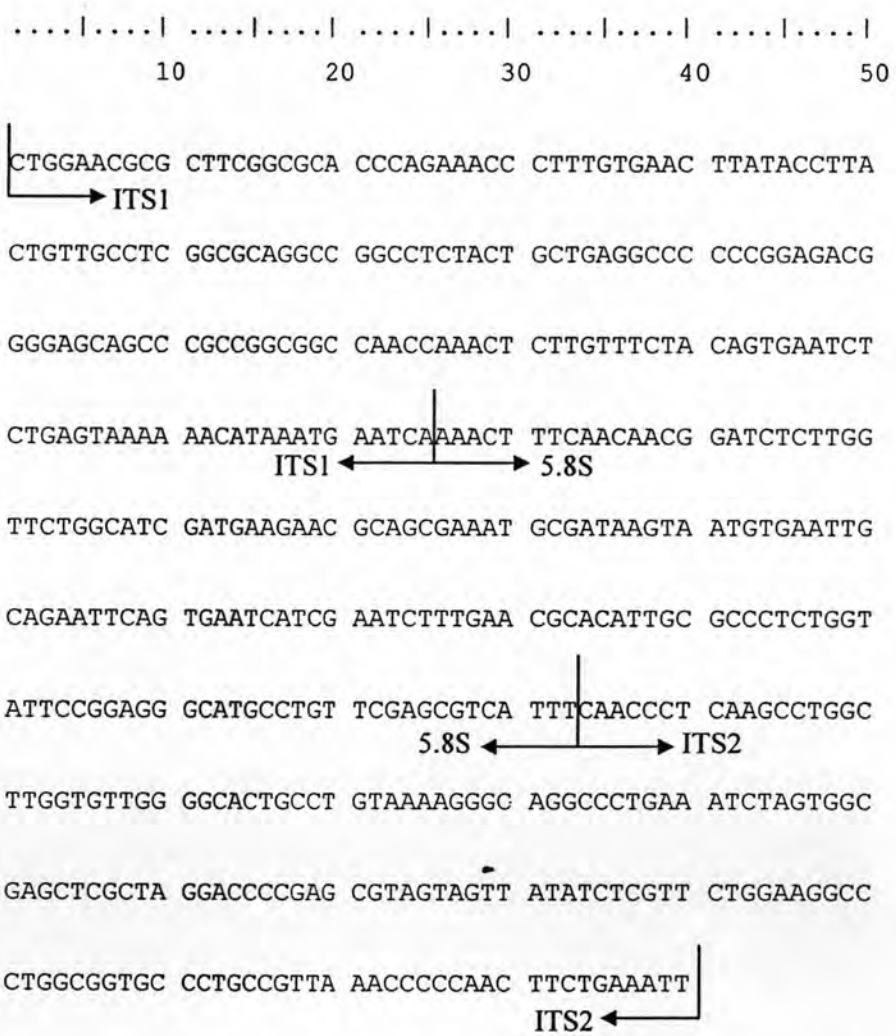

Figure 4.14 Nucleotide sequences of the ITS1-5.8S-ITS2 regions of rDNA of endophytic fungal isolate HANT 7.

4.4.2.2 Phylogenetic analysis

The search for similar sequences to complete ITS1-5.8S-ITS2 sequence of HANT 7 from GenBank DNA databases revealed that the ITS1-5.8S-ITS2 region of endophytic fungus isolate HANT 7 had relatively sequence similarity to *Diaporthe helianthi* with 97% identity. The isolate HANT 7 also had relatively high nucleotide similarity with 96% identity to that of *Phomopsis columnaris*, *Phomopsis glabrae*, *Diaporthe phaseolorum*, and *Phomopsis vexans*. Another 13 reference taxa showed 92-95 % identity as shown in Table 4.12. These results confirmed that HANT 7 was found to be in the clade of *Phomopsis* sp. and its teleomorph, *Diaporthe* sp.

The phylogenetic relationship inferred from these data is shown in Figure 4.15. This inferred phylogenetic tree was 50% majority rule consensus trees with 300 steps tree length, with consistency index (CI), retention index (RI) and rescaled consistency index (RC) of 0.7000, 0.5313, and 0.3719, respectively.

Table 4.12 The alignment scores (% identity) of complete ITS1-5.8S-ITS2 sequences of the isolate HANT 7 and 15 reference taxa from GenBank.

HANT 7															
96	***P. columnaris***														
96	95	***P. glabrae***													
96	94	95	***D. conorum***												
97	95	96	97	***D .helianthi***											
96	93	95	96	96	***D. phaseolorum***										
95	94	94	96	96	94	***D. angelicae***									
95	94	94	96	97	94	97	***D. arctii***								
95	94	95	95	96	95	94	94	***P. chimonanthi***							
95	94	95	95	96	95	94	94	100	***P. micheliae***						
93	91	92	92	92	91	92	93	91	91	***P. liquidambari***					
95	94	95	95	96	97	94	94	96	96	90	***P. camptothecae***				
95	94	95	95	97	97	94	94	96	96	91	99	***D. melonis***			
95	94	95	95	96	97	94	94	96	96	90	100	99	***D. sojae***		
92	91	91	91	92	90	92	93	91	91	95	91	91	91	***D. eres***	
96	93	94	96	96	95	96	95	94	94	92	95	95	95	91	***P. vexans***

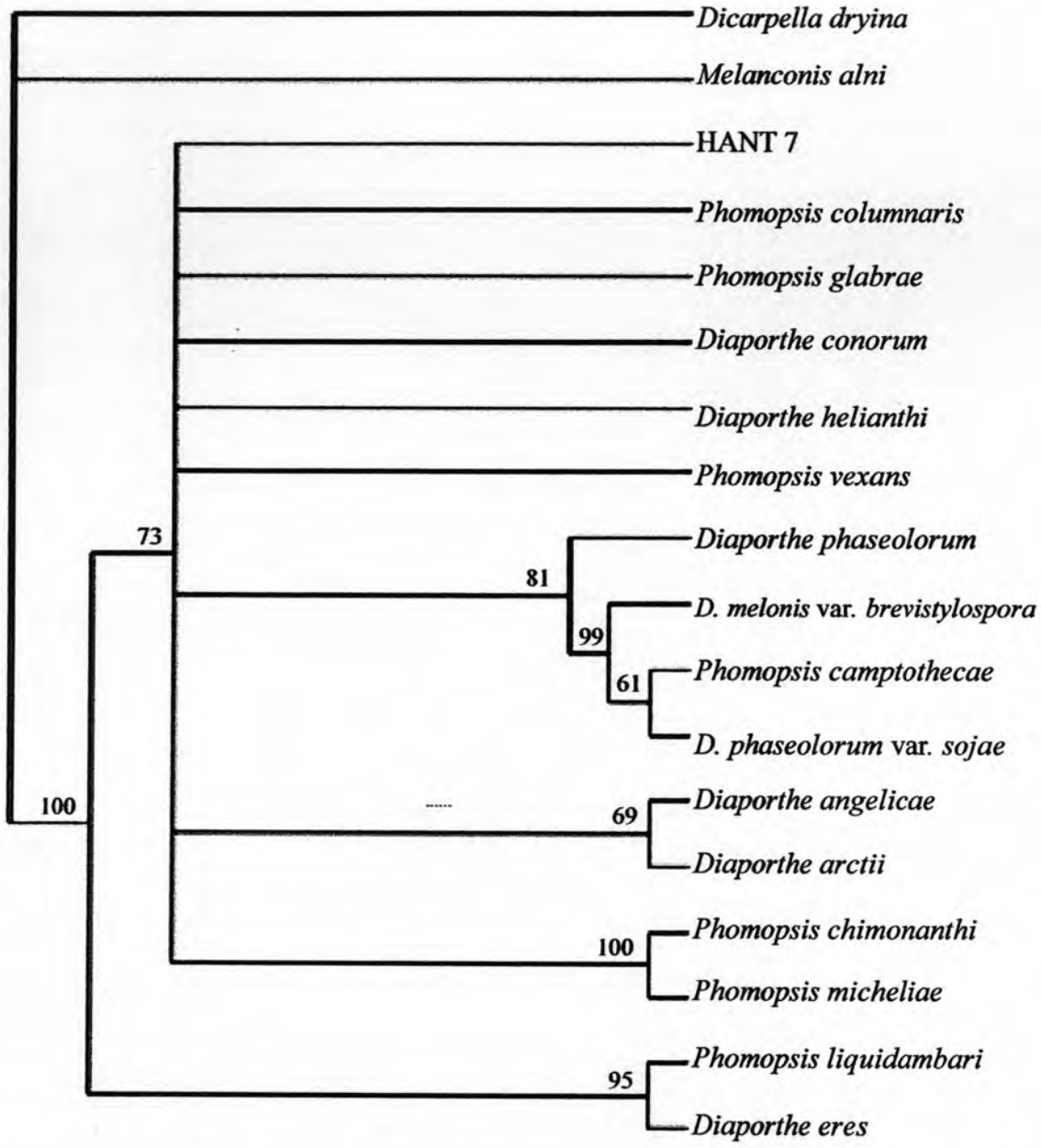

Figure 4.15 Maximum-parsimony tree (50% majority-rule consensus tree) generated from the ITS1-5.8S-ITS2 sequences of 18 taxa [consistency index = 0.7, retention index = 0.5313, rescaled consistency index = 0.3719, tree length = 300 steps) showing the evolutionary relationship of HANT 7 with reference taxa. The numbers at internal node indicate the percentages of trees from 1,000 bootstrap replications. *Dicarpella dryina* and *Melanconis alni* were used as outgroups.

4.4.2.3 Nucleotide sequence of complete ITS1-5.8S-ITS2 sequence of HANT 25

The PCR sequencing of ITS1-5.8S-ITS2 sequence of the isolate HANT 25 (amplified with the conserved fungal primer ITS_5 and ITS_4) was done by the Bioservice Unit (BSU), the National Center for Genetic Engineering and Biotechnology (BIOTEC). The isolate HANT 25 produced a complete ITS1-5.8S-ITS2 sequence. The length of corresponding fragment was 513 bp, as shown in Figure 4.16.

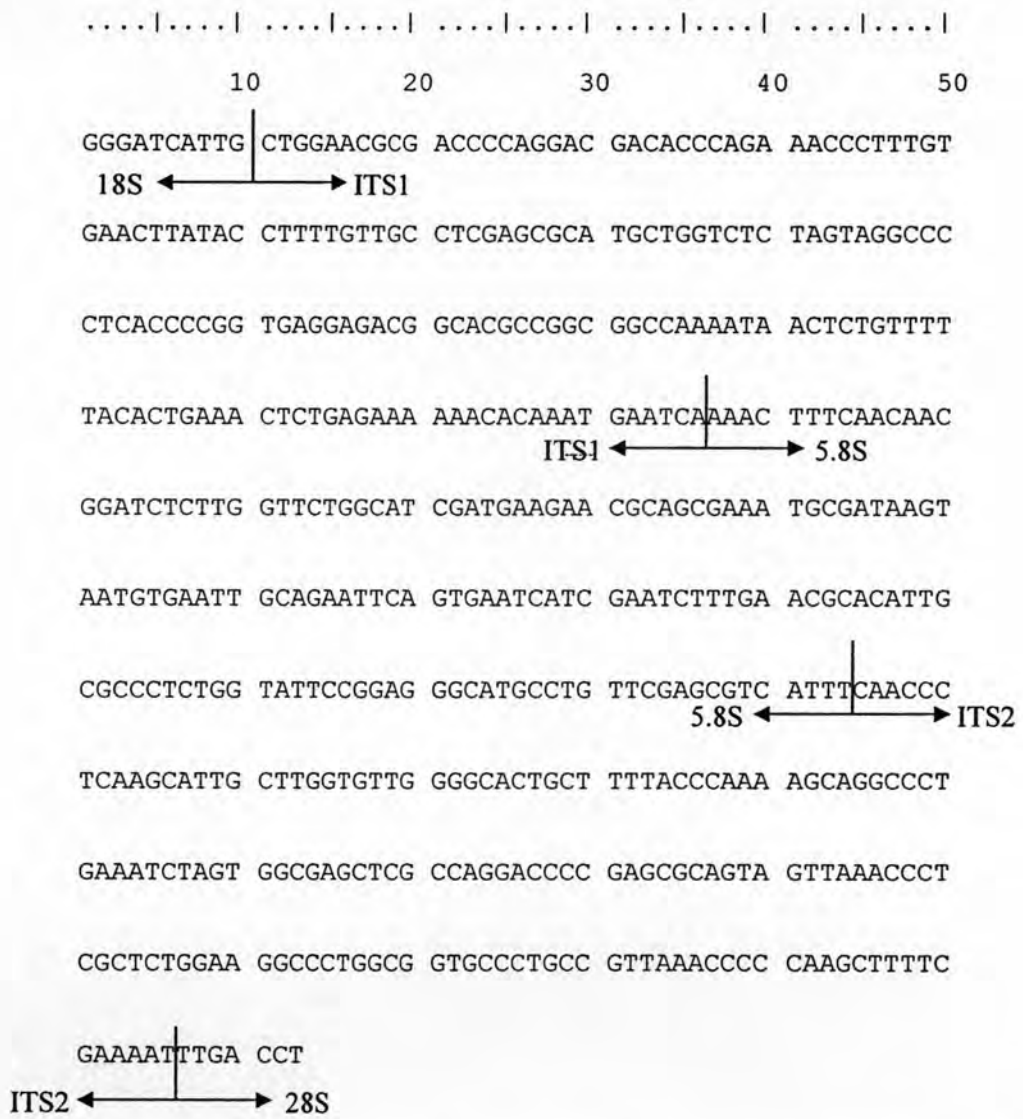

Figure 4.16 Nucleotide sequences of the partial 18S sequence, complete ITS1-5.8S-ITS2 and partial 28S sequence of rDNA of endophytic fungal isolate HANT 25.

4.4.2.4 Phylogenetic analysis

A blast search was performed to find a similar sequence to the ITS1-5.8S-ITS2 region of the fungal isolate HANT 25 in the Genbank DNA database, available from: http://0-www.ncbi.nlm.nih.gov.library.vu.edu.au/BLAST/. The results revealed that the ITS region of the endophytic fungal isolate HANT 25 had relatively higher sequence similarity to *P. bougainvilleicola* and *P. oryzae* with 97% identity than with any other sequence. The isolate HANT 25 also had relatively high nucleotide similarity with 96% identity to that *D. phaseolorum* and *P. averrhoae.* The isolate HANT 25 also had relatively high sequence similarities with nine *Phomopsis* sp. and seven *Diaprothe* sp. (91-95% identity) as shown in Table 4.13. These results confirmed that HANT 25 is *Phomopsis* sp. and its teleomorph, *Diaporthe* sp.

The phylogenetic relationship inferred from these data is shown in Figure 4.17. This inferred phylogenetic tree was 50% majority rule consensus trees with 281 steps tree length, with consistency index (CI), retention index (RI) and rescaled consistency index (RC) of 0.7260, 0.7775, and 0.5644, respectively. Evolution of HANT 25 was found to be most closely related to with 75% bootstrap support, as shown in Figure 4.17.

Table 4.13 The alignment scores (% identity) of complete ITS1-5.8S-ITS2 sequences of the isolate HANT 25 and 20 reference taxa from GenBank.

HANT 25																			
97	*P. bougainvilleicola*																		
96	98	*D. phaseolorum*																	
96	97	98	*P. averrhoae*																
97	97	97	98	*P. oryzae*															
95	96	95	96	97	*D. arctii*														
93	94	94	96	94	94	*P. phyllanthicola*													
93	94	94	95	94	94	99	*P. loropetali*												
93	95	95	95	94	93	97	97	*P. lagerstroemiae*											
93	94	95	95	95	93	98	97	99	*P. eucommii*										
92	94	94	94	94	93	96	96	98	98	*P. asparagi*									
92	93	93	93	93	92	92	92	93	92	92	*P. quercina*								
92	93	93	93	93	92	92	92	92	92	92	99	*P. amygdali*							
92	94	93	93	94	92	93	93	93	93	92	99	99	*P. magnoliae*						
91	93	92	92	93	91	91	92	92	92	91	99	99	99	*P. juniperivora*					
92	94	93	93	93	92	93	93	93	93	92	98	98	98	98	*D. helianthi*				
91	93	92	93	93	91	93	92	93	93	92	98	98	98	97	97	*D. vaccinii*			
92	93	93	93	93	92	93	92	93	93	92	98	98	98	97	97	99	*P. vaccinii*		
91	93	93	94	94	93	95	95	96	95	95	95	95	96	95	95	95	95	*P.eucommicola*	
91	93	93	94	93	93	95	95	95	95	94	95	95	95	94	95	95	95	99	*P. conorum*
91	92	91	93	92	92	94	94	95	95	94	95	95	96	95	95	95	95	99	99	*P. melonis*

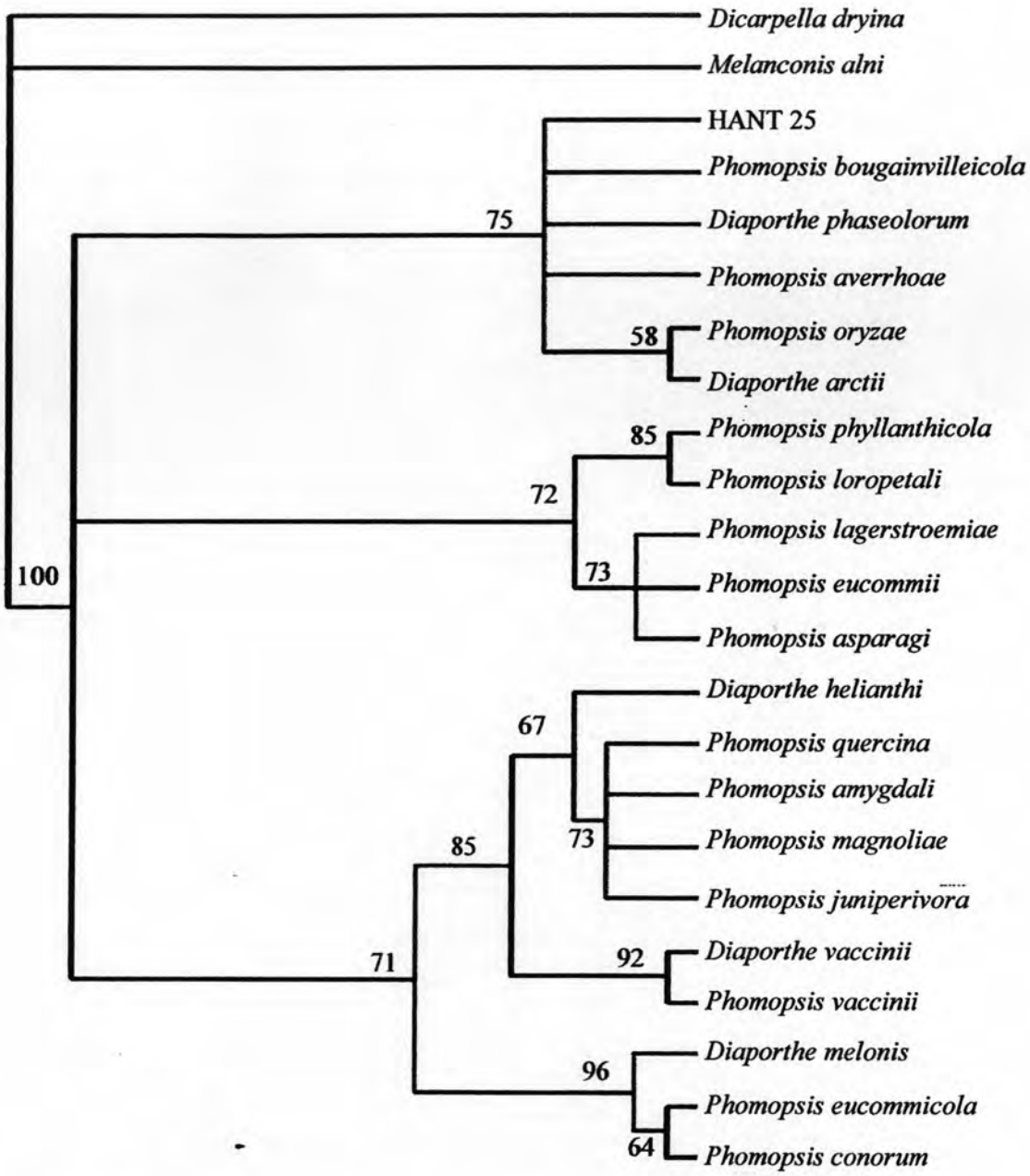

Figure 4.17 Maximum-parsimony tree (50% majority-rule consensus tree) generated from the ITS1-5.8S-ITS2 sequences of 23 taxa [consistency index (CI) = 0.7260, retention index (RI) = 0.7775, rescaled consistency index (RC) = 0.5644, tree length = 281 steps] showing the evolutionary relationship of HANT 25 with reference taxa. The numbers at internal node indicate the percentages of trees from 1,000 bootstrap replications. *Dicarpella dryina* and *Melanconis alni* were used as outgroups.

4.5. Biological activity

4.5.1 Cytotoxic activity of compounds 1, 2, 3, and 4

The in vitro cytotoxic activity of compounds **1** and **4** from the endophytic fungal isolates HANT 25 and HANT 7 against 12 cell lines is summarized in Table 4.14. Compounds **2** and **3** were evaluated for cytotoxic activity against 3 cell lines as summarized in Table 4.15.

Table 4.14 Cytotoxic activity of compounds **1** and **4**.

Cytotoxicity	Compound		Etoposide (positive control)
	1	4	
HuCCA-1	0.30	30.00	3.00
KB	2.40	>50 (Inactive)	0.30
HeLA	2.10	>50 (Inactive)	0.25
MDA-MB231	1.30	33.00	0.15
T47D	2.00	29.00	0.02
H69AR	1.60	>50 (Inactive)	27.00
HepG2	2.25	>50 (Inactive)	0.18
A549	1.95	>50 (Inactive)	0.55
S102	2.80	>50 (Inactive)	0.52
HL-60	0.85	25.10	1.30
P388	0.80	15.30	0.19
Vero cell	4.36	ND	-

Table 4.15 Cytotoxic activity of compounds **2** and **3**.

Name	Cytotoxicity activity [IC_{50} (μg/mL)]		
	HepG2	**A549**	**S102**
Compound **2**	1.45	1.70	0.87
Compound **3**	>50 (Inactive)	>50 (Inactive)	>50 (Inactive)
Etoposide (positive control)	17.00	21.00	>50

HuCCA-1	Human cholangiocarcinoma
KB	Human epidermoid carcinoma in mouth
HeLA	Human cervical carcinoma
MDA-MB231	Hormone-independent breast cancer
T47D	Hormone-dependent breast cancer
HepG2	Human hepatoblastoma carcinoma
H69AR	Lung cancer, small cell, multidrug resistance
A549	Human lung cancer, non small cell
S102	Hepatocellular carcinoma
HL-60	Human promyelocytic leukemia cell
P388	Mouse lymphoid neoplasm

As shown in Table 4.14, compound **1** exhibited strong cytotoxic activity against HuCCA-1, H69AR, and HL-60 cell lines with IC_{50} values of 0.30, 1.60, and 0.85 μg/mL, respectively. Compound **1** also exhibited cytotoxic activity against other seven cell lines including, KB, HeLA, MDA-MB231, T47D, HepG2, A549, S102, and P388 cell lines with respective IC_{50} values of 2.40, 2.10, 1.30, 2.00, 2.25, 1.95, 2.80, and 0.80 μg/mL. However, compound **1** exhibited relatively strong cytotoxic activity against the Vero cell with IC_{50} value of 4.36 μg/mL. Compound **4** exhibited weak cytotoxic activity against HuCCA-1, MDA-MB231, T47D, HL-60, and P388 cell lines with IC_{50} values of 30.00, 33.00, 29.00, 25.10, and 15.30 μg/mL, respectively.

As shown in Table 4.15, compound **2** exhibited strong cytotoxic activity against HepG2, A549, and S102 cell lines with IC_{50} values of 1.45, 1.70, and 0.87 μg/mL, respectively. Compound **3** was found inactive against HepG2, A549, and S102 cell lines.

Compounds **1** and **2** showed cytotoxicity, while **3** was inactive. Compound **3** contains dehydrogenation of C-2/C-3 double bond which may cause inactivity towards cell lines. Therefore the α,β-unsaturated δ-lactone ring in **1** and **2** has a significant effect on cytotoxicity.

4.5.2 Antimicrobial activity of compounds 1 and 4

Compound **1** was found to exhibit activity against *Mycobacterium tuberculosis* (MIC value 50 μg/mL), but inactive toward other activities tested. Compound **4** was found inactive against the malarial parasite. The bioactivity results of compounds **1** and **4** are summarized in Table 4.16.

Table 4.16 Antimicrobial activity of compounds **1** and **4**.

Compound	**Anti-HSV-1** IC_{50} (μg/mL)	**Antifungal** IC_{50} (μg/mL)	**Anti-TB** MIC (μg/mL)	**Anti-malarial**
1	Inactive	Inactive	50	Inactive
4	ND*	ND*	ND*	Inactive

*ND = Not determine

4.5.3 Antioxidant, anti-inflammation and anti-estrogenicity activity of compounds 1 and 4

Compound **1** was found to exhibit antioxidant activity [inhibition of TPA-induced $O_2^{\cdot -}$ generation differentiated HL-60 cell (HL-60 Antiox.)] with IC_{50} 14.9 μM. The bioactivity results of compounds **1** and **4** are summarized in Table 4.17.

Table 4.17 Antioxidant, anti-inflammation and anti-estrogenicity activity of compounds **1** and **4**.

Compound	Antioxidant					Anti-inflammation	Anti-estrogenicity
	DPPH $IC_{50}(\mu M)$	**HL-60 Antiox.** $IC_{50}(\mu M)$	**NXO** $IC_{50}(\mu M)$	**IXO** $IC_{50}(\mu M)$	**ORAC** (Unit)	**LOX** IC_{50} (μM)	**AIA** IC_{50} (μM)
1	>250	14.9	>500	>500	0.8	>100	>12.5
4	>250	>100	>500	>500	1.2	>100	>12.5

DPPH	Scavenging of diphenyl picrylhydrazyl radicals
HL-60 Antiox.	inhibition of TPA-induced $O_2^{\cdot -}$ generation differentiated HL-60 cell
NXO or XXO	Scavenging of $O_2^{\cdot -}$ generating by xanthine/xanthine oxidase
IXO	Inhibition of xanthine oxidase
ORAC	Oxygen radical absorbance capacity (against $ROO^{\cdot}$)
LOX	Inhibition of lipoxygenase activity
AIA	Inhibition of aromatase activity